



Experimental and theoretical study of 10-methoxy-2-phenylbenzo[h]quinoline

Dong Zhenming^a, Shi Heping^a, Liu Yufang^a, Liu Diansheng^a, Liu Bo^{b,*}

^a School of Chemistry and Chemical Engineering, Shanxi University, Taiyuan 030006, China

^b Institute of Chemistry, School of Science Beijing Jiaotong University, Beijing 100044, China

ARTICLE INFO

Article history:

Received 7 September 2010

Received in revised form

20 November 2010

Accepted 17 December 2010

Keywords:

10-Methoxy-2-phenylbenzo[h]quinoline

Crystal structure

Absorption spectra

Emission spectra

TDDFT

ABSTRACT

10-Methoxy-2-phenylbenzo[h]quinoline (MPBQ) has been synthesized and characterized by NMR and X-ray single crystal diffraction. Both the ground and the lowest singlet excited-state geometries of MPBQ were optimized by B3LYP and ab initio CIS methods at 6-31G (d,p) level, respectively. The absorption and emission spectra of the compound were experimentally determined in CH₃CN solution and were simultaneously computed using density functional theory (DFT) and time-dependent density functional theory (TDDFT) in CH₃CN solution. The calculated absorption and emission wavelengths were in good agreement with the experimental ones. The calculated lowest-lying absorption spectra can be mainly attributed to intramolecular charge transfer (ICT). And the calculated fluorescence spectra can be mainly described as originating from an excited state with intramolecular charge transfer (ICT) character. These results show that MPBQ exhibited excellent thermal stability and could serve as a useful photoluminescence material.

© 2010 Elsevier B.V. All rights reserved.

1. Introduction

10-Hydroxybenzo[h]quinoline (HBQ) is a fused heterocyclic compound that contains a phenol group. Both phenol group and the fused aromatic rings are accessible for chemical modifications, making further derivations of HBQ feasible. Owing to their great potential applications in the field of organic light emitting devices (OLEDs), HBQ and its derivatives have been extensively investigated during the past years [1–16]. The photophysical properties of this class of compounds can be modified readily by derivatization. Thus, the development of new materials for organic EL devices with high performance constitutes a very active area of research. Recently, a series of new HBQ derivatives have been synthesized as efficient emitting materials in organic EL devices and their photophysical properties have been investigated in detail [17–21]. In addition to experimental approaches, the density functional theory (DFT) as well as the time-dependent density functional theory (TDDFT) have been widely used for studying the electronic structures and spectral properties of HBQ and HBQ derivatives, generating highly accurate results [22–25].

Herein, we report the synthesis of a novel BHQ derivative 10-methoxy-2-phenylbenzo[h]quinoline as well as its crystal structure, electronic structure and spectral properties. We also attempt to elucidate the structure–property correlation of this molecule. Our results show that MPBQ exhibited excellent ther-

mal stability and could serve as a useful photoluminescence material.

2. Experimental

2.1. Reagents

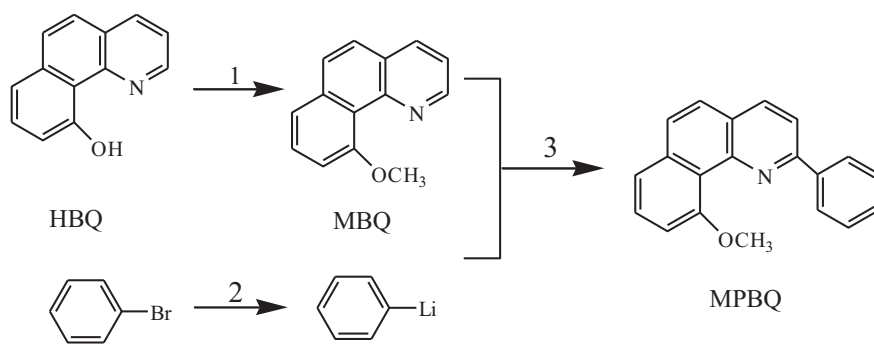
10-Hydroxybenzo[h]quinoline (HBQ) is prepared according to the reported procedures [1]. n-Butyllithium and 2-bromobenzene were purchased from Alfa Aesar and used as received. Dimethyl sulfate, tetrahydrofuran, hexane, and benzene etc. were treated according to standard methods. All the reactions were carried out under nitrogen atmosphere unless otherwise mentioned.

2.2. Apparatus

Melting points were determined on an x-5 melting point detector and were uncorrected. ¹H and ¹³C NMR spectra were obtained on a Bruker 300 MHz instrument in CDCl₃. Elemental analyses were performed with an Elementar Analysensysteme (GmbH). Thermal stability was assessed with a TA Instruments model 2050 thermogravimetric analyzer under N₂. The temperature range used was from room temperature to 350 °C at a heating rate of 20 °C/min. Mass spectra were recorded with the LC–MS system consisted of a Waters 1525 pump and a Micromass ZQ4000 singlequadrupole mass spectrometer detector (Waters). The single crystal X-ray diffraction data were collected on a Bruker SMART CCD area-detector diffractometer. UV–vis spectra were obtained on a Shimadzu UV-2450 spectrophotometer. Fluorescence spec-

* Corresponding author. Tel.: +86 10 6226 9413.

E-mail address: liubo4314@yahoo.com.cn (L. Bo).



Reagents: 1, $\text{Me}_2\text{SO}_4, \text{KOH}, 1,4\text{-dioxane}$; 2, $n\text{-BuLi}, n\text{-hexane-THF}$; 3, $n\text{-hexane-THF}$.

Scheme 1. The synthetic route of MPBQ.

tra were obtained on a Shimadzu RF-5301PC spectrofluorometer. All spectral experiments were carried out at room temperature. Excitation and emission slit widths were both set at 5 nm.

2.3. Synthesis and characterization of MPBQ

The synthetic route to MPBQ is shown in Scheme 1.

2.3.1. Synthesis of 10-methoxybenzo[h]quinoline (MBQ)

HBQ (4.88 g, 25.0 mmol) was added to a suspension of KOH (1.69 g, 30.0 mmol) in 1,4-dioxane (30 mL). After the KOH powder and HBQ were dissolved, a solution of dimethyl sulfate (3.16 g, 25.0 mmol) in 1,4-dioxane (15 mL) was added portionwise with stirring at room temperature. After stirring for 10 h, the reaction mixture was filtered to remove the solid residue. The filtrate was poured into 1000 mL of water and then was made basic with Na_2CO_3 to give the crude product MBQ as a yellow precipitate (4.5 g). The crude product was collected by filtration, washed well with an ethanol–water mixture (1/1 v/v), and recrystallized from benzene by gradually adding n-hexane to give MBQ as a yellow powder (3.0 g; yield: 61.5% based on HBQ).

2.3.2. Synthesis of 10-methoxy-2-phenylbenzo[h]quinoline (MPBQ)

Under a nitrogen atmosphere and at -78°C , a solution of n-butyllithium (0.16 mol) in anhydrous n-hexane (100 mL) was added portionwise with stirring to a solution of 2-bromobenzene (8.8 g, 56.3 mmol) in anhydrous tetrahydrofuran (100 mL), and stirring continued for 50 min to form 2-lithiophenoxide. Afterwards, a solution of MBQ (7.85 g, 37.5 mmol) in tetrahydrofuran (75 mL) was added dropwise with stirring over 2 h and the mixture was stirred for another 3 h. The resulting orange reaction mixture was poured over 400 g crushed ice and neutralized with 6 M HCl solution, and then the organic solvents, n-hexane and tetrahydrofuran, were removed by evaporation to give the crude product MPBQ as a dark-red solid (11.1 g). The crude product was collected by filtration and then washed well with a hot ethanol–water mixture (1/1 v/v). Finally, recrystallization from benzene gave a pure sample of MPBQ as an orange powder (3.7 g; yield 42.0% based on MBQ). Pale yellow block single crystals of MPBQ suitable for X-ray diffraction were obtained by crystallization from a concentrated solution of benzene at room temperature. Mp $160\text{--}163^\circ\text{C}$. $^1\text{H NMR}$ (300 MHz, CDCl_3) δ : 8.43 (d, 2H), 8.40 (d, 1H), 8.20 (d, 1H), 7.54–7.76 (m, 6H), 7.44 (d, 1H), 7.26 (d, 1H), 4.25 (s, 3H). $^{13}\text{C NMR}$ (300 MHz, CDCl_3) δ : 161.612, 157.085, 149.303, 142.097, 138.640, 131.316, 131.012, 130.542, 130.269, 129.537, 128.208, 123.423, 119.479, 112.201, 58.949, MS (m/z): 285 (M^+). Anal. Calcd. for $\text{C}_{20}\text{H}_{15}\text{NO}$: C, 84.19; H, 5.30; N, 4.91 O, 5.61. Found: C, 83.79; H, 5.33; N, 4.89; O, 5.63.

The thermal stability of MPBQ was measured using thermogravimetric analysis (TGA). The result revealed that MPBQ exhibited excellent thermal stability up to 250°C .

2.3.3. Crystal structural determination

A pale yellow block crystal with approximate dimensions of $0.30\text{mm} \times 0.20\text{mm} \times 0.20\text{mm}$ was selected for data collection. Reflection data were measured at 273 K using graphite-monochromated Mo/ $\text{K}\alpha$ radiation ($\lambda = 0.71073 \text{ \AA}$). The ω - 2θ scan technique was used with θ limit $2.3^\circ < \theta < 25^\circ$. The structure was solved by direct methods using the SHELXTL program package. All the non-hydrogen atoms were refined on F2 anisotropically by full-matrix least squares methods. All the hydrogen atoms were placed in calculated positions assigned fixed isotropic thermal parameters at 1.2 times the equivalent isotropic U of the atoms to which they are attached and allowed to ride on their respective parent atoms. The contributions of these hydrogen atoms were included in the structure-factor calculations [26–28].

2.4. Computational methods

All calculations were performed using Gaussian 03 program [29]. The geometry optimizations of the electronic ground state (S_0) were carried out at the DFT level [30,31] with the hybrid B3LYP exchange–correlation functional [32,33], and the split-valence 6-31G(d,p) basis set [34]. DFT/B3LYP/6-31G(d,p) has been found to be an accurate formalism for calculating the structural properties of many molecular systems [35]. No symmetry constraints were imposed during the optimization process. Frequency calculations were carried out to ensure that the geometries obtained corresponded to minima and not saddle points.

The methodology to determine the singlet–singlet excitation energies was the adiabatic approximation to the time dependent density functional theory (TDDFT) approach [36], using a B3LYP hybrid functional and a 6-31G(d,p) basis set. A polarizable continuum (PCM) model has been applied for the solvent effects as implemented in Gaussian 03 [37–39]. In this work, we have used the keyword (solvent = CH_3CN). The equilibrium structure of the first singlet excited states (S_1) has been optimized using the restricted CIS (RCIS) theoretical method with the 6-31G(d,p) basis set [40]. Emission energies were obtained from TDDFT/B3LYP/6-31G(d,p) calculations performed on S_1 optimized geometries. Solvent effects were also taken into account by the PCM model applied to the equilibrium approximation in the TDDFT calculations. All the calculations have been performed using the advanced computing facilities of supercomputing center of computer network information center of Chinese Academy of Sciences.

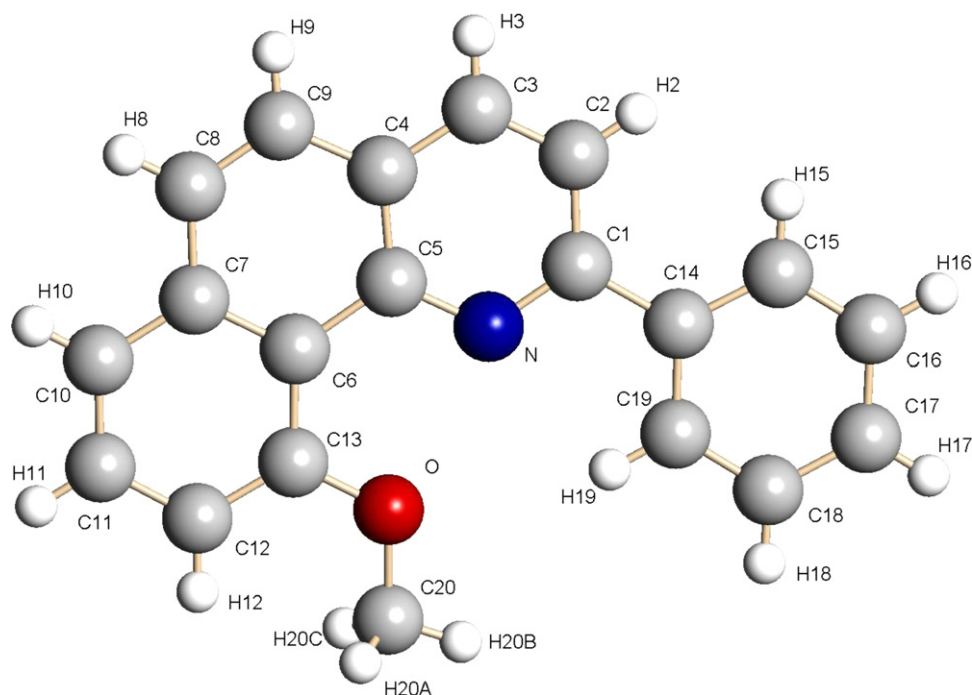


Fig. 1. The crystal structure of MPBQ.

3. Results and discussion

3.1. Molecular structure

The crystal structure of MPBQ was determined by X-ray diffraction and crystal data for the title compound are given in Table S1 in the Supporting Information. The crystal structure of MPBQ is shown in Fig. 1. And the crystal structure parameters are listed in Table 1. As shown in Table 1, MPBQ contains one molecule in the asymmetric unit. The molecule adopts a planar conformation in crystal structure. The torsion angles of N–C(1)–C(14)–C(19) and C(2)–C(1)–C(14)–C(19) are $1.2(2)^\circ$ and $-178.59(15)^\circ$, respectively.

The geometry of MPBQ in the ground state was optimized using the DFT/B3LYP/6-31G (d, p) method. The optimized structure is shown in Fig. 2. The values of the parameters are listed in Table 1. As can be seen from the data of Table 1, MPBQ has an asymmetrically distorted geometrical structure. The dihedral angles of C(23)–C(25)–C(34)–N(35) and C(23)–C(25)–C(34)–C(30) are 17.5° and -161.5° , respectively.

3.2. Frontier molecular orbitals and spectral properties

3.2.1. Frontier molecular orbitals

The frontier molecular orbitals can provide a reasonable qualitative indication of the excitation properties and the ability of

electron or hole-transport [41]. The energies of the HOMO and LUMO orbitals of MPBQ were investigated at the DFT/B3LYP/6-31G (d,p) level. Fig. 3 shows the isodensity surface plots of HOMO and LUMO. It can be seen from Fig. 3 that the electron density of HOMO is mainly localized on the phenol ring and it is π -bonding orbitals. And the electron density of LUMO is mainly localized on the pyridine ring and it is π^* -bonding orbitals. The electronic transition from the ground state to the excited state is mainly about electron flowing from the phenol ring including O to the pyridine ring including N, which belongs to π – π^* transition. In Table 2 we present the energies of the HOMO and LUMO as well as the HOMO–LUMO energy gap. In order to further understand the electron transport ability, we optimized the geometry of the anionic MPBQ. The optimized structure for the anion shows small structural changes relative to the neutral molecule. On the basis of the small structural relaxation, we expected that this system would exhibit a relatively high structural stability versus the injection of one negative charge. Finally we calculated vertical and adiabatic ionization potential (IP_V and IP_A) as well as vertical and adiabatic electron affinity (EA_V and EA_A), and the results are shown in Table S2 in the Supporting Information. Electron affinities can be viewed as the variations of energy adding an electron. The negative electron affinities here implied that adding an electron to the molecule would release some energy. Thus, this system has a better electron transport property.

Table 1

The structure parameters of MPBQ.

Crystal parameters			Optimized parameters		
Bond lengths	C(1)–C(2)	1.404(2)	Bond lengths	R(15,25)	1.4042
	C(1)–C(14)	1.485(2)		R(23,25)	1.4054
	C(14)–C(15)	1.385(2)		R(25,34)	1.4887
	C(14)–C(19)	1.387(2)		R(30,34)	1.4162
Bond angles	N–C(1)–C(14)	115.39(15)	Bond angles	A(15,25,34)	122.1639
	C(2)–C(1)–C(14)	122.86(16)		A(23,25,34)	119.407
	C(15)–C(14)–C(1)	122.71(16)		A(25,34,30)	121.784
	C(19)–C(14)–C(1)	119.80(16)		A(25,34,35)	116.3944
	N–C(1)–C(14)–C(15)	$-178.36(15)$		D(15,25,34,30)	18.6709
Torsion angles	N–C(1)–C(14)–C(19)	$1.2(2)$	Dihedral angles	D(15,25,34,35)	-162.3229
	C(2)–C(1)–C(14)–C(15)	$1.8(3)$		D(23,25,34,30)	-161.4933
	C(2)–C(1)–C(14)–C(19)	$-178.59(15)$		D(23,25,34,35)	17.5128

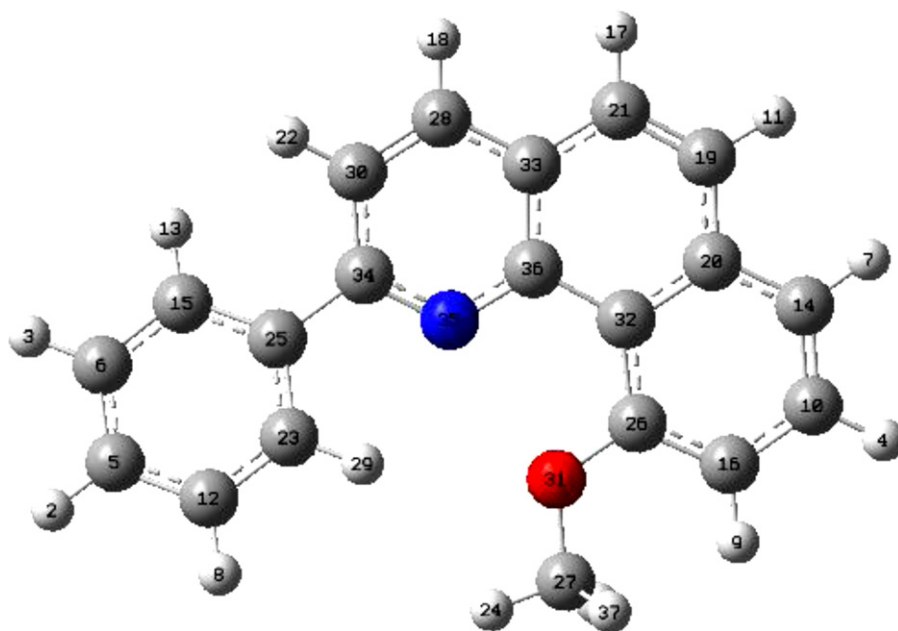


Fig. 2. The optimized structure of MPBQ molecule in the ground state.

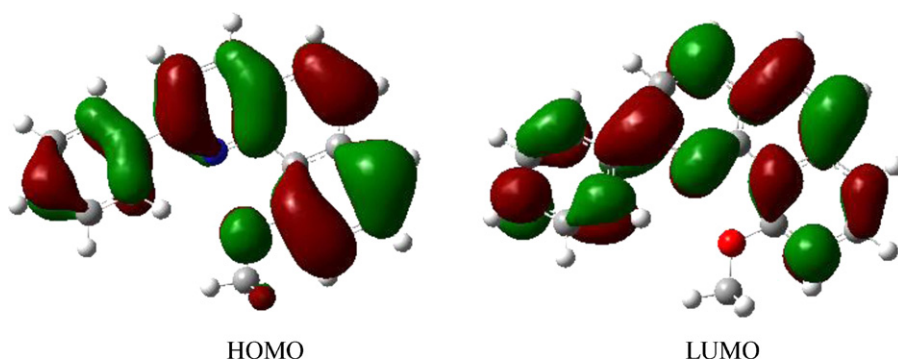


Fig. 3. Isodensity surface plots for the frontier orbitals of MPBQ in the ground state.

3.2.2. UV-vis spectra

The UV-vis spectra of MPBQ obtained in CH_3CN solution are shown in Fig. 4. The spectra were normalized with respect to the maximum peak. It is seen that MPBQ exhibited two absorption bands at 353 and 371 nm, which could be attributed to the π - π^* electronic transitions. Besides, the energy of the higher absorption peak at $28,328\text{ cm}^{-1}$ agreed with the calculated energy for the $S_0 \rightarrow S_1$ excitation.

To provide insight into the nature of the UV-vis absorption observed experimentally for the compound, we computed the singlet-singlet electronic transitions using TDDFT method at the B3LYP/6-31G(d, p) level on the optimized geometry in the ground state (S_0) in CH_3CN , yielding the vertical electronic transitions of $S_0 \rightarrow S_1$. The data are shown in Table 3. As can be seen from Table 3, the electronic transitions were of the π - π^* type. The calculated $S_0 \rightarrow S_1$ excitation energy of the compound in CH_3CN solution is $28,210\text{ cm}^{-1}$ and its oscillator strength is 0.3386. This electronic transition is allowed and it is generated mainly from the HOMO to

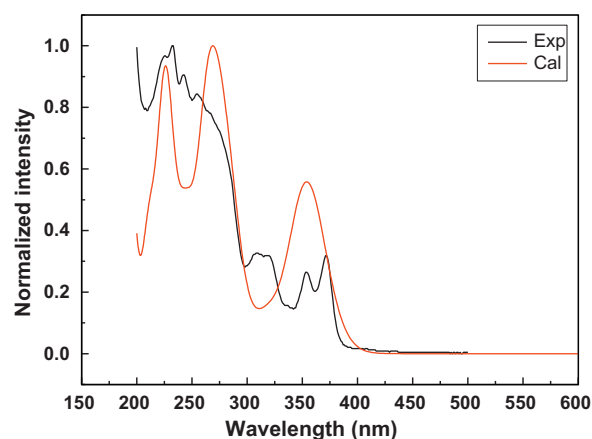


Fig. 4. Experimental and calculated absorption spectra of MPBQ in CH_3CN .

Table 2

The frontier orbitals energies of MPBQ in the ground state.

Orbital	Energy	Energy gaps
HOMO(75)	-5.388	4.024
LUMO(76)	-1.361	

Table 3

The calculated absorptions of MPBQ using the TDDFT method at B3LYP level.

Wavelength λ_{max} (nm)	Excitation energies (eV)	Oscillator strengths	MO/character	Transition
354.48	3.497	0.3386	75- \rightarrow 760.65001	$S_1 \leftarrow S_0$
			74- \rightarrow 770.13867	

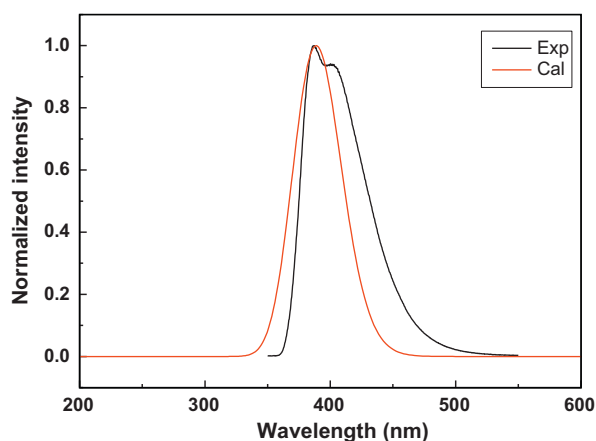


Fig. 5. Experimental and calculated emission spectra of MPBQ in CH₃CN.

Table 4
Fluorescence spectral data of MPBQ in CH₃CN solvent.

Emission energy (cm ⁻¹)	Emission wavelength (nm)	Stokes shift (cm ⁻¹)	MO/character	Transition
25,906	386	2422	LUMO ← HOMO	S ₁ → S ₀
24,875	402	2079		

LUMO. The absorption peak at the longest wavelength is assigned to the electronic transition from HOMO to LUMO according to the calculation in CH₃CN solvent. It can be assigned to π - π^* transition with intramolecular charge transfer (ICT) character. On the basis of the calculated vertical excitation energies and their corresponding oscillator strengths, the continuous absorption spectrum was simulated with the help of SWIZARD software with the width at half-height of 2500 cm⁻¹. As shown in Fig. 4, the simulated absorption spectrum is in relatively good agreement with the measured spectrum of the compound.

3.2.3. Fluorescence spectra

Fig. 5 shows the normalized fluorescence spectrum of MPBQ in CH₃CN solution excited at 353 nm. The spectrum consists of two emission bands with peaks at 386 and 402 nm attributed to the π - π^* electronic transitions. Values of the emission peak energy and Stokes shifts are given in Table 4. The higher energy peak in the emission spectrum occurs at 25,906 cm⁻¹ with small Stokes shift, which can be assigned to the S₁ → S₀ electronic transition.

In order to gain insight into the nature of the fluorescence emission observed for MPBQ, the geometry of the first excited singlet state (S₁) was optimized for the compound. The optimized geometry of the S₁ state were used as input in the TDDFT method to obtain the electronic transition energies from the relaxed excited states to the ground state in CH₃CN solution. The data are listed in Table 5. The electronic transitions were of the π - π^* type. The calculated S₁ → S₀ emission energy of the compound in CH₃CN solution was 25,723 cm⁻¹ and its oscillator strength was 0.5161. This transition was also allowed. Moreover, TDDFT calculations gave small Stokes

Table 5
The calculated fluorescence emission of MPBQ using the TDDFT method at B3LYP level.

Emission wavelength λ_{\max} (nm)	Emission energy (eV)	Oscillator strengths	MO/character	Transition
388.75	3.1893	0.5161	74 → 760.10725 75 → 760.64670	S ₁ → S ₀

shift, as a consequence of the similar geometries in the S₀ and S₁ states. It was 2487 cm⁻¹ in CH₃CN solution. As shown in Table 5, the emission peak of MPBQ can be described as originating from π - π^* excited states with ICT character. On the basis of the calculated vertical excited energies and their corresponding oscillator strengths, the continuous emission spectrum was simulated with the help of SWIZARD software with the width at half-height of 2500 cm⁻¹. As shown in Fig. 5, the simulated emission spectrum is in relatively good agreement with the experimental fluorescence spectrum of the compound. The maximum emission wavelengths of MPBQ are 386 and 402 nm in CH₃CN solution.

4. Conclusions

In this paper, a new benzo[h]quinoline derivative, namely, 10-methoxy-2-phenylbenzo[h]quinoline (MPBQ) was synthesized and characterized by NMR, MS as well as elemental analysis. The single-crystal X-ray crystallographic analysis indicated that MPBQ adopts a planar conformation in crystal structure and contains one molecule in the asymmetric unit. The absorption and fluorescence spectra of MPBQ in CH₃CN calculated by quantum chemistry computations were in good agreement with the experimental data. With good thermal stability, MPBQ could be potentially used as an excellent luminescent material. Such studies are currently under way in our laboratory, and the results will be released soon.

Acknowledgements

All the calculations have been performed using the advanced computing facilities of supercomputing center of computer network information center of Chinese Academy of Sciences. All the authors express their deep thanks.

Appendix A. Supplementary data

Supplementary data associated with this article can be found, in the online version, at doi:10.1016/j.saa.2010.12.067.

References

- [1] H. Schenkel, M. Schenkel, *Helv. Chim. Acta* 27 (1944) 1456–1463.
- [2] C.T. Bruice, *J. Am. Chem. Soc.* 79 (1957) 702–705.
- [3] H. Okawa, M. Ikeguchi, T. Yoshino, *Ser. C: Chem.* 5 (1966) 149–153.
- [4] M.L. Martinez, W.C. Cooper, P.T. Chou, *Chem. Phys. Lett.* 193 (1992) 151–154.
- [5] E.L. Roberts, P.T. Chou, T.A. Alexander, R.A. Agbaria, I.M. Warner, *J. Phys. Chem.* 99 (1995) 5431–5437.
- [6] A.I. Sytnik, J.C. Del Valle, *J. Phys. Chem.* 99 (1995) 13028–13032.
- [7] M. Kubicki, T. Borowiak, W.Z. Antkowiak, *Acta Crystallogr. C: Cryst. Struct. Commun.* 51 (1995) 1173–1175.
- [8] P.T. Chou, C.Y. Wei, *J. Phys. Chem.* 100 (1996) 17059–17066.
- [9] D. LeGourrierec, V. Kharlanov, R.G. Brown, W. Rettig, *J. Photochem. Photobiol. A: Chem.* 117 (1998) 209–216.
- [10] P.T. Chou, C.Y. Wei, W.S. Yu, Y.H. Chou, *J. Phys. Chem. A* 105 (2001) 1731–1740.
- [11] X.S. Wu, H.S. Sun, Y. Pan, H.B. Chen, X.Z. Sun, *Chin. Chem. Lett.* 10 (1999) 875–878.
- [12] H. Matsumiya, H. Hoshino, T. Yotsuyanagi, *Analyst* 126 (2001) 2082–2086.
- [13] P.T. Chou, G.R. Wu, Y.I. Liu, W.S. Yu, *J. Phys. Chem. A* 106 (2002) 5967–5973.
- [14] H. Matsumiya, H. Hoshino, *Anal. Chem.* 75 (2003) 413–419.
- [15] Y. Qiu, J. Qiao, *CN Patent 1388205, Chem. Abstr.* 140, 2003.
- [16] S. Takeuchi, T. Tahara, *J. Phys. Chem. A* 109 (2005) 10199–10207.
- [17] H.R. Hyeon, H.J. Ji, K.K. Young, K.H. Yun, *Curr. Appl. Phys.* 6 (2006) 712–717.
- [18] K.Y. Chen, C.C. Hsieh, Y.M. Cheng, C.H. Lai, P.T. Chou, *Chem. Commun.* 42 (2006) 4395–4397.
- [19] Z.Q. Guo, Z.M. Dong, R.T. Zhu, S. Jin, B. Liu, *Acta Part A* 68 (2007) 337–340.
- [20] C.H. Kim, T. Joo, *Phys. Chem. Chem. Phys.* 11 (2009) 10266–10269.
- [21] D.C. Powers, D. Benitez, E. Tkatchouk, W.A. Goddard, *J. Am. Chem. Soc.* 132 (2010) 14092–14103.
- [22] J. Carlos, D. Valle, *J. Chem. Phys.* 270 (2001) 1–12.
- [23] C. Schriever, K. Stock, A.J.A. Aquino, D. Tunega, *Chem. Phys.* 347 (2008) 446–461.
- [24] J.A. Aquino, F. Adelia, M. Plasser, Barbatti, H. Lischka, *Croat. Chem. Acta* 82 (2009) 105–114.
- [25] H.P. Shi, L. Xu, X.F. Zhang, L.Q. Jiao, Y. Cheng, J.Y. He, J.X. Yao, L. Fang, C. Dong, *J. Mol. Struct.: Theochem.* 950 (2010) 53–63.

- [26] G.M. Sheldrick, Correction Software, University of Gottingen, Germany, 1996.
- [27] Sheldrick, Program for the Solution of Crystal Structures, University of Gottingen, Germany, 1997.
- [28] Program for Crystal Structure Refinement, Bruker Analytical X-ray Instruments Inc., Madison, Wisconsin, USA, 1998.
- [29] M.J. Frisch, G.W. Trucks, H.B. Schlegel, G.E. Scuseria, M.A. Robb, J.R. Cheeseman, J.A. Montgomery, T. Jr. Vreven, K.N. Kudin, J.C. Burant, J.M. Millam, S.S. Iyengar, J. Tomasi, V. Barone, B. Mennucci, M. Cossi, B. Scalmani, G.N. Rega, G.A. Petersson, H. Nakatsuji, M. Hada, M. Ehara, K. Toyota, R. Fukuda, J. Hasegawa, M. Ishida, T. Nakajima, Y. Honda, O. Kitao, H. Nakai, M. Klene, X. Li, J.E. Knox, H.P. Hratchian, J.B. Cross, C. Adamo, J. Jaramillo, R. Gomperts, R.E. Stratmann, O. Yazyev, A.J. Austin, R. Cammi, C. Pomelli, J.W. Ochterski, P.Y. Ayala, K. Morokuma, G.A. Voth, P. Salvador, J.J. Dannenberg, V.G. Zakrzewski, S. Dapprich, A.D. Daniels, M.C. Strain, O. Farkas, D.K. Malick, A.D. Rabuck, K. Raghavachari, J.B. Foresman, J.V. Ortiz, Q. Cui, A.G. Baboul, S. Clifford, J. Cioslowski, B.B. Stefanov, G. Liu, A. Liashenko, P. Piskorz, I. Komaromi, R.L. Martin, D.J. Fox, T. Keith, M.A. Al-Laham, C.Y. Peng, A. Nanayakkara, M. Challacombe, P.M.W. Gill, B. Johnson, W. Chen, M.W. Wong, C. Gonzalez, J.A. Pople, Gaussian, Inc., Pittsburgh PA, 2003.
- [30] P. Hohenberg, W. Kohn, Phys. Rev. 136 (1964) B864–B871.
- [31] W. Kohn, L.J. Sham, Phys. Rev. 140 (1965) A1133–A1138.
- [32] A.D. Becke, J. Chem. Phys. 98 (1993) 5648–5652.
- [33] C. Lee, W. Yang, R.G. Parr, Phys. Rev. B 37 (1988) 785–789.
- [34] R. Ditchfield, W.J. Hehre, J.A. Pople, J. Chem. Phys. 54 (1971) 724–728.
- [35] S. Tretiak, S. Mukamel, Chem. Rev. 102 (2002) 3171–3212.
- [36] E. Gross, J. Dobson, M. Petersilka, Top. Curr. Chem. 181 (1996) 81–172.
- [37] M. Cossi, N. Rega, G. Scalmani, V. Barone, J. Chem. Phys. 114 (2001) 5691–5701.
- [38] B. Mennucci, J. Tomasi, R. Cammi, J.R. Cheeseman, M.J. Frisch, F.J. Devlin, S. Gabriel, P.J. Stephens, J. Phys. Chem. A 106 (2002) 6102–6113.
- [39] M. Cossi, G. Scalmani, N. Rega, V. Barone, J. Chem. Phys. 117 (2002) 43–54.
- [40] J.B. Foresman, M. Head-Gordon, J.A. Pople, M.J. Frisch, J. Phys. Chem. 96 (1992) 135–149.
- [41] M. Belletete, J.F. Morin, M. Leclerc, G. Durocher, J. Phys. Chem. A 109 (2005) 6953–6959.